Phononic Crystals for Suppressing Crosstalk in Ultrasonic Flowmeters

Sabiju Valiya Valappil, Johannes F. L. Goosen, and Alejandro M. Aragón

***Abstract*— Ultrasonic flowmeters that use transit-time ultrasonic transducers face measurement errors due to "crosstalk," whereby the working signal travels through the pipe wall and couplings, interfering with the signal from the fluid. Although various procedures have been proposed to solve the issue of crosstalk, they're limited to low-frequency ranges, or they are not effective in high-pressure environments. We propose a mounting mechanism based on a single-phase 3-D phononic crystal (PnC) waveguide that can mitigate crosstalk at high frequencies (megahertz range) and thus improve the flowmeters' measurement accuracy. PnCs are artificial materials consisting of periodically arranged scatterers thereby showing bandgaps (BGs)—ranges of frequencies where elastic/acoustic waves are attenuated—due to Bragg scattering. We design PnC wave filters by engineering the BG frequency range to the working signal of the ultrasonic flowmeter. We then fabricate the waveguide using additive manufacturing and connect it between the transducer and the pipe wall. Transient ultrasonic experiments show that transducers with PnC mountings attain a 40 dB crosstalk reduction in comparison with a standard transducer mounting configuration.**

***Index Terms*— Band gap, band structure, finite element analysis (FEA), metal additive manufacturing, phononic crystals (PnCs), transient experiments, transmissibility, ultrasonic flowmeters, ultrasonic transducers, wave attenuation.**

I. Introduction

ULTRASONIC transducers, due to their versatility and nondestructive nature, are extensively used in various measurement systems, including ultrasonic flowmeters [1], [2], [3], [4], nondestructive testing devices [5], [6], [7], and medical imaging systems [8], [9], [10]. These transducers convert electrical input signals to ultrasound waves (and vice versa), which interact with the desired media to provide the required measurement. However, ultrasonic flowmeters that use transit-time ultrasonic transducers to measure flow rates through pipes face accuracy issues due to "crosstalk," which is caused by the interference of signals traveling through the solid region (solid/pipe signal) with the fluid region (fluid signal). In addition, the solid signal contains more energy than the required signal due to the often unavoidable large impedance mismatch between the transducer, pipe wall, and the measuring fluid, leading to an immense reflection of waves in the solid portion. Hence, crosstalk makes it difficult to identify the required signal [11].

Various solutions have been proposed to mitigate crosstalk in ultrasonic flowmeters. For instance, crosstalk has been minimized by isolating the sensor from the solid signal path [12]. For example, enclosing the acoustic transducer and the surrounding housing in a sheath also aids in isolating the housing from the rest of the solid region, thereby minimizing the interaction between the solid and fluid signals [13]. Another approach is to create time delays between the required and the pipe signals [14]. For instance, applying protrusions to transducers increases the solid wave path so that the solid signal arrives at the receiving transducer after the fluid signal, thus avoiding the crosstalk [15]. A third approach is by localizing the energy transmitted from the pipe signal [16]. To that end, resonators and damping systems are attached to the transducer [17], where resonators aid in localizing the energy while damping systems reduce the energy of solid waves by converting the wave energy to heat.

All these methods, however, have drawbacks. In the case of the protruded design, the distance between the transducers determines the generation of the crosstalk. For example, if the transducers are far away, as in the case of a large-diameter pipe, then the solid signal could arrive at the receiver along with the required signal resulting in crosstalk. This distance limitation imposes restrictions on the pipe diameter, flow velocity, and sound velocity of the fluid medium, among others [18], [19]. Resonators and damping systems are limited to relatively low frequencies (a few hundred kilohertz) because it is difficult to construct an oscillator that has resonance frequencies in the megahertz-range at the macroscale. Similarly, damping systems with constant dissipation are also less effective at high frequencies because, although energy increases with the frequency, the dissipation remains the same. Acoustic insulation becomes an issue in high-pressure environments since a heavy casing is needed to withstand high pressures, which increases the crosstalk by allowing more solid waves to pass through the casing [20]. Consequently, for the smooth operation of the flowmeter, it is necessary to have a wave filtering mechanism that removes the crosstalk, which has a substantial operational frequency range (at megahertz level) and has a limited influence from pressure and temperature.

A potential solution could be based on frequency-dependent insulation by exploiting the properties of phononic crystals

Manuscript received 12 October 2022; revised 26 April 2023; accepted 16 May 2023. Date of publication 27 June 2023; date of current version 5 July 2023. This work was supported in part by the Topconsortia voor Kennis en Innovatie (TKI) Project Grant and in part by Krohne. The Associate Editor coordinating the review process was Dr. Yong Yan. *(Corresponding author: Alejandro M. Aragón.)*

The authors are with the Department of Precision and Microsystems Engineering, Faculty of Mechanical, Maritime and Materials Engineering, Delft University of Technology, 2628 CD Delft, The Netherlands (e-mail: a.m.aragon@tudelft.nl).

This article has supplementary downloadable material available at https://doi.org/10.1109/TIM.2023.3284960, provided by the authors.

Digital Object Identifier 10.1109/TIM.2023.3284960

(PnCs) [21], [22], [23]. PnCs are man-made periodic media that exhibit Bragg scattering [24] type band gaps (BGs)—ranges of frequencies where elastic/acoustic waves are attenuated. Because of BGs, PnCs have been explored in many applications, including vibration isolation [25], energy harvesting [26], acoustic cloaking [27], super/hyper lens [28], [29], frequency steering [30], among others. PnCs (or similar periodic structures) have previously been used inside the piezoelectric component of transducers to optimize the piezoelectric coefficient [31], [32], [33], [34]. Another related application of PnCs in ultrasonic transducers is to improve the measurement accuracy of the transducers in nondestructive evaluation [35], [36]. Liu et al. [37] used PnCs to improve the sensitivity of acoustic-ultrasonic-based devices for structural health monitoring, thereby improving their performance for a broad frequency range. By blocking unwanted signals using PnCs, Kabir et al. [38] were able to enhance the crack detection ability of the acoustic emission method [39]. Other applications of PnCs in ultrasonic transducers include enhancing sound receiving accuracy of parametric loudspeakers [40], and reducing nonlinearities in ultrasonic damage detection [41]. Still, to the best of our knowledge, PnC structures have not been used as mountings on the transducer of ultrasonic flowmeters to mitigate crosstalk.

In this article, we investigate the use of PnC structures as wave filters to mitigate crosstalk in ultrasonic flowmeters (Fig. 1). A PnC-embedded wave filter is designed, realized, and connected between the piezo and the back of the transducer that is attached to the pipe wall such that the PnC waveguide filters the signal arriving from the pipe wall to the piezo. We explore various practical aspects, such as selecting the geometry and arrangement of the PUCs for the best performance within a limited space and choosing a suitable material for the mounting. In addition, we incorporate manufacturing aspects and industrial standards in the design process. We fabricate two different designs of PnC waveguides via additive manufacturing, where one has a broad BG frequency, and the other possesses greater manufacturability. For comparison purposes, we also construct a dummy block with the exact outer dimensions as the PnC waveguide via the same manufacturing process (additive manufacturing). We validate the performance of the PnC-embedded ultrasonic transducer via transient ultrasonic experiments and compare them against a standard transducer.

II. Theoretical Aspects of Ultrasonic Transducers and PnCs

A. Challenges in the Flow Measurement Through a Pipe Using an Ultrasonic Flowmeter

The flow rate through a pipe can be measured by various methods such as pressure-based meters, variable-area type measurement systems, optical systems, magnetic flowmeters, Coriolis devices, and ultrasonic flowmeters [42]. Among them, ultrasonic flowmeters are of great interest because of their high accuracy and low maintenance cost [43]. In an ultrasonic flowmeter, a high-frequency ultrasound pulse generated using an ultrasonic transducer (based on piezoelectric effect [44]) is transmitted through the moving media at an angle. An ultrasonic receiver receives this signal on the opposite side, which provides the travel time. The exact process is repeated in the reverse direction resulting in an upstream and downstream measurement. The difference between these two signals' travel times is directly related to the flow rate through the pipe. Several transmitters and receivers can be placed along the circumference of the pipe to further improve the measurement accuracy, which, in addition, also aids in obtaining a flow profile through the pipe. The layout and operation of the ultrasonic flowmeter are provided in Fig. 1.

TABLE I
Material Properties of the Pipe and Fluid

Material	Density ($\mathrm{kg/m^3}$)	Pressure wave speed, C_P ($\mathrm{m\,s^{-1}}$)	Shear wave speed, C_S ($\mathrm{m\,s^{-1}}$)
Stainless steel	7800	4935.5	3102.9
Water	998.2	1481.4	–

The figure shows the cross-sectional [Fig. 1(a)] and longitudinal-sectional [Fig. 1(c)] views of the pipe with ultrasonic transducers, along with a photograph of the transducer [Fig. 1(b)]. The ultrasonic transducer mainly comprises a piezoceramic material (Piezo) for converting electric pulse to ultrasound and vice versa and a window [a structural element usually constructed of the same material as the pipe that is in contact with the fluid, which is marked in Fig. 1(b)] for transmitting this pulse to the fluid and receiving it at the opposite side. The transducer also possesses electrical components for supplying and receiving electric signals. A metallic casing (stainless steel in the present case) encloses the transducer for protection. Due to its complex construction and the presence of multiple materials, various challenges may occur during the flow measurement that could hinder the flowmeter's accuracy.

The 1 MHz input pulse [refer to Fig. 1(a)] generated at the transmitter arrives at the window-fluid interface and experiences an immense reflection due to the considerable mismatch in the impedance (density $\times$ speed of sound) between the window and the fluid layer (refer Table I for the material properties of the pipe and the fluid).

This reflected signal travels through the solid portion (red signal path in Fig. 1) to reach the receiver, thus interfering with the required signal (green signal path). This interaction of the two signals (crosstalk) is a complex phenomenon because it comprises pressure waves (P waves) from the fluid region and pressure and shear waves (S waves) from the solid region. Due to crosstalk, the measured signal experiences a reduction in accuracy or even the complete loss of the working signal [45]. Thus, to avert crosstalk, a mechanism is necessary that prevents both P and S wave propagation in the solid region from reaching the receiving transducer. In addition, as the flowmeter (and the transducer) will be exposed to high-pressure and temperature environments, the mounting

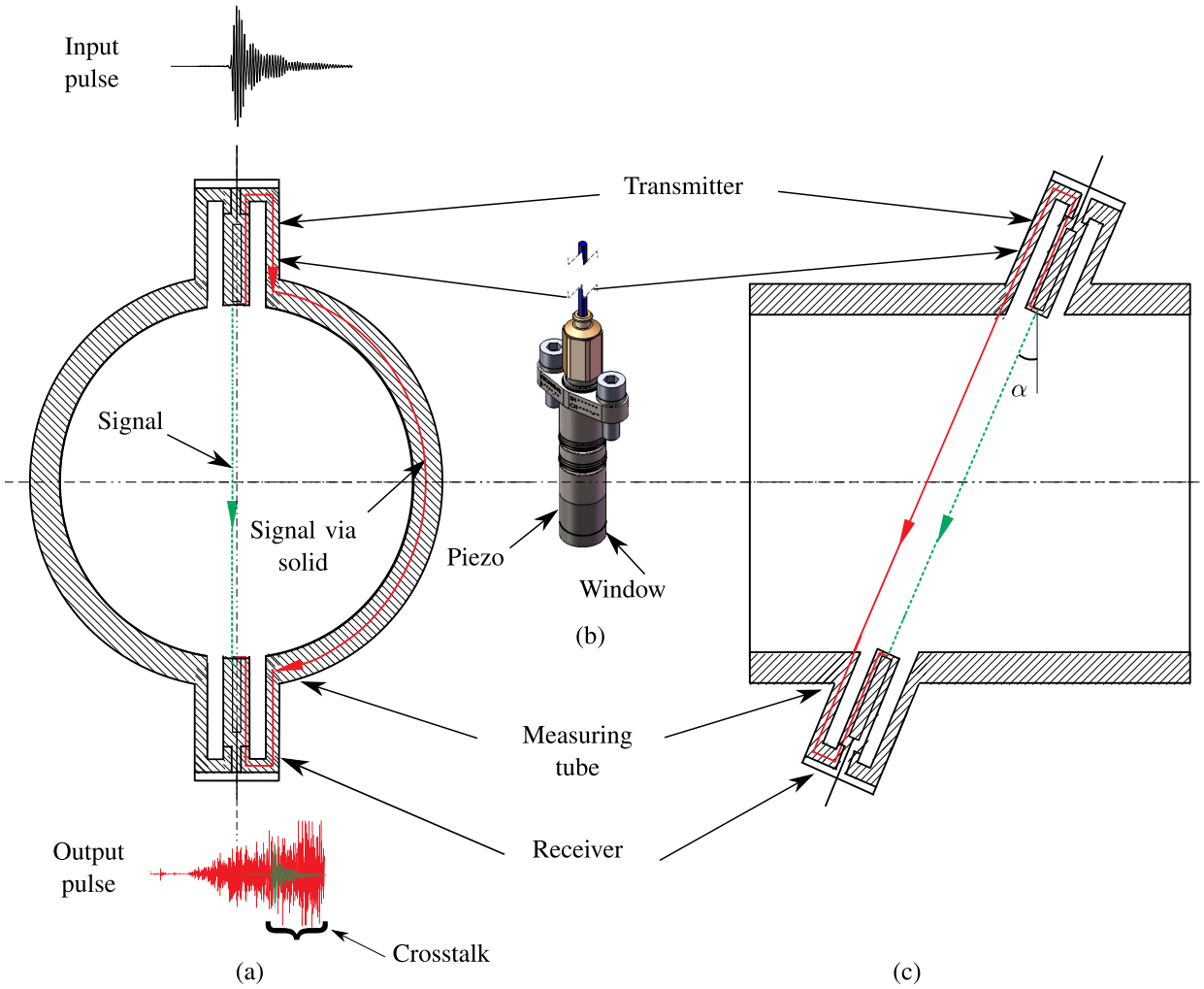

Fig. 1. Schematic of the ultrasonic flowmeter, where (a) shows its cross-sectional view highlighting the signal paths through the fluid and the solid media. Input pulse and output pulse with crosstalk are also shown here, where the signal through the solid region (red plot) arrives much earlier than the signal through the fluid (green plot), resulting in the crosstalk between these signals (marked using a curly bracket in the output pulse). (b) Photographs of an actual ultrasonic transducer where the Piezo generates the pulse and the window that transmits the signal to the fluid are marked using arrows. (c) Longitudinal section of the flowmeter with transmitting and receiving transducers and signal and noise paths. The transmitter and receiver are oriented at an angle α to enable the flow measurement.

mechanism should be able to prevent or reduce crosstalk under these conditions.

B. Design Requirements for the Mounting Structure

Since crosstalk is a significant issue in an ultrasonic flowmeter, we would like to address it by filtering out the solid (pipe wall) signal. As mentioned already, by attaching a mounting structure in the solid wave path that would act as a mechanical wave filter, we might be able to remove the solid signals for the desired frequency range. Since the ultrasonic transducer is composed of stainless steel 316 (SS316), we could fabricate the mounting system from the same material, ensuring a smooth contact and energy transfer between the transducer and the mounting. As the transducer signal is broadband (1 MHz central frequency with a bandwidth of 600 kHz), it is also necessary for the mounting structure to possess a wide operating frequency range with its central frequency close to 1 MHz. Moreover, the lateral dimension of the mounting structure should be in a similar range to that of the outer diameter of the transducer (18 mm). Finally, the structure should be manufacturable at a reasonable cost.

C. PnC-Based Mounting Mechanism

As PnCs possess BGs that can attenuate incoming waves for particular frequency ranges, we design a mounting mechanism based on a single-phase 3-D PnC waveguide. To investigate wave propagation through the 3-D PnC structure, we need the corresponding wave equation. Since the PnC waveguide is entirely composed of solid material, the wave propagation is governed by the 3-D elastic wave equation

$$\rho \ddot{\boldsymbol{u}} = (\lambda + 2\mu)\Delta \boldsymbol{u} - \mu \nabla \times \nabla \times \boldsymbol{u} \tag{1}$$

where $\boldsymbol{u}$ and $\ddot{\boldsymbol{u}}$, respectively, are the spatial displacement and the acceleration. ρ represents the density of the material, λ and μ are the Lamé coefficients, whereas Δ and $\nabla \times$, respectively, represent Laplacian and vector curl operators.

We still need to provide the necessary boundary conditions to fully define the boundary value problem (BVP). We study two BVPs, for which the BCs are as follows.

1) *BVP1 (Band Structure Analysis):* (or dispersion analysis) [46] establishes the relationship between the applied frequency ω and the wave vector $\boldsymbol{k}$ that provides the BG frequency range (if any) and speeds of different wave modes. The magnitude of the wave vector $\boldsymbol{k}$ is the reciprocal of the wavelength and it is directed toward the direction of the wave propagation (i.e., in the direction of the phase velocity) [47]. The dispersion relation is obtained by conducting a set of eigenvalue analyses of the periodic unit cell (PUC) after applying Bloch–Floquet periodic boundary conditions (BFPBCs) [48] through the irreducible Brillouin zone (IBZ) [49]. The Brillouin zone (BZ) is derived by transforming the PUC from the direct lattice (Bravais lattice [50]) to its reciprocal lattice [51]. The IBZ is the smallest section of the BZ that can capture the wave dynamics of the PUC. We consider a simple cubic PUC [as shown in Fig. 2(a), (b), (d), and (e)] with a 32-fold symmetry, thus the BZ could be reduced to a tetrahedron (as shown in Fig. 2(c)) [52]. The number of eigenvalue analyses conducted depends on the sampling of the wave vector through the IBZ, as we need one analysis per wave vector step. Similarly, the number of eigenmodes selected for the analysis depends on the frequency range of interest. Since we are interested in the megahertz range, we started with 30 eigenmodes. The BFPBC used in these analyses takes the form

$$\boldsymbol{u}(\boldsymbol{r}+\boldsymbol{a}_i,t)=e^{\iota \boldsymbol{k}.\boldsymbol{a}_i}\boldsymbol{u}(\boldsymbol{r},t) \tag{2}$$

where $\boldsymbol{r}$ is the position vector and $\boldsymbol{a}_i$ is the lattice vector in 3-D, i.e., $\boldsymbol{a}_i=\{\boldsymbol{a}_1,\boldsymbol{a}_2,\boldsymbol{a}_3\}$ [refer Fig. 2(a)]. For the cubic geometry, magnitudes of lattice parameters are the same in all three directions, i.e.,

$$\|\boldsymbol{a}_1\|=\|\boldsymbol{a}_2\|=\|\boldsymbol{a}_3\|=a \tag{3}$$

where a is the magnitude of the lattice vector (in any of the three directions). If no wave vectors are present for a range of frequencies implying no wave propagation for that frequency range, we get a BG. In addition, we can obtain wave speeds for various wavebands by taking slopes of the dispersion relation corresponding to those wavebands. Although less expensive (due to operating on one PUC), the band structure analysis assumes an infinite medium by prescribing BFPBC. Thus, it cannot provide an actual attenuation rate for a finite PnC structure, so we need a transmissibility analysis.

2) *BVP2 (Transmissibility Analysis):* (or harmonic frequency sweep analysis) [53] is the steady-state dynamic analysis of the finite PnC waveguide after applying the essential (Dirichlet) boundary condition [54]

$$\boldsymbol{u}(\boldsymbol{l},t)=\bar{\boldsymbol{u}}e^{\iota\omega t} \tag{4}$$

where $\bar{\boldsymbol{u}}$ is the constant displacement amplitude applied at one end (left end) of the PnC waveguide (at $\boldsymbol{r}=\boldsymbol{l}$), [shown in Fig. 2(f) and (g)] and ω is the applied frequency. For a given frequency, the transmissibility response provides the reduction in amplitude of the input signal for a given number of PUCs arranged in space.

III. Design and Analysis of PnC-Based Wave Filter

Using the band structure and transmissibility analyses, we can start the design process of PnC's PUC and waveguide. Since the BGs in PnCs are generated due to Bragg scattering, we can use Bragg's law of diffraction to obtain the size of the PUC as follows [24]:

$$n\bar{\lambda}=2a\cos\theta \tag{5}$$

where n is an integer, $\bar{\lambda}$ is the wavelength in the material, and θ is the angle of incidence of the wave to the normal of the surface. At $n=1$, for a normal incident wave, the magnitude of the lattice parameter can be half of the wavelength in the medium. We can obtain the wavelength in the material from the following expression:

$$\bar{\lambda}=C/f \tag{6}$$

where f is the applied frequency and C is the wave speed. $C=C_P$ for pressure waves and $C=C_S$ for shear waves. For our material choice, SS316, the wave speed values are provided in Table I. To design a PUC possessing a BG with a central frequency of 1 MHz, we can use (5) and (6) to obtain the magnitude of the lattice parameter, which is estimated to be 2 mm. To accommodate a broad operational frequency range (600 kHz), the PnC should possess a broad BG. We know that the BG width is directly related to the contrast in adjacent phases' impedances within the PUC [55]. Since we have a single-phase PUC, to maximize the impedance mismatch within the elements of the PUC, we need to maximize the contrast in their masses and stiffnesses [56]. Based on literature and understanding of dynamics, we chose large spheres separated by small rods, as shown in Fig. 2(a) and (b), to construct the PUC. There is about an order difference in the cross-sectional area of the sphere to the rod. On the contrary, while the second one [refer to Fig. 2(d) and (e)] has triangular features instead of spherical ones that offer lower contrast in the properties than the former—resulting in narrower BG—the manufacturability is greatly improved by minimizing overhang angles in additive manufacturing. By populating the PUCs in three dimensions, we arrive at PnC waveguide designs that are shown in Fig. 2(f) and (g). We also add two hollow cylindrical fixtures to connect them to the transducer from Fig. 1(b). To verify the performance of these PUCs and waveguides we perform band structure and transmissibility analyses.

A. Band Structure Response

The band structure of the cubic PnC is obtained through finite element analysis (FEA) by following the $\omega(\boldsymbol{k})$ approach [56], i.e., by sweeping the wave vector along the vertices of the IBZ and calculating the set of eigenfrequencies corresponding to a fixed number of wavebands. Fig. 3(a) and (b), respectively, represent the band structures of PUCs with spherical and triangular features (their geometries are shown in Fig. 2). These figures show frequency as a

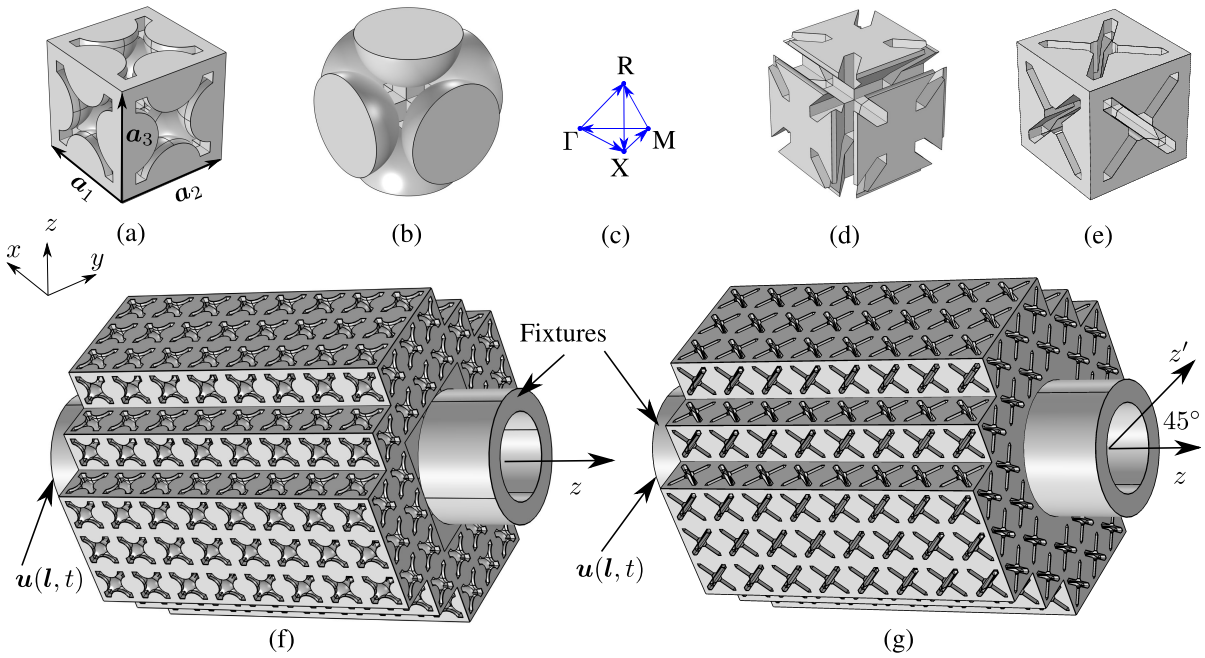

Fig. 2. Three-dimensional PnC PUCs and waveguides where (a) and (b) show different views of the cubic PUC with spherical features where $\boldsymbol{a}_i$ ($i = 1$ to 3) defines its lattice parameter. (c) IBZ of the cubic PUC. (d) and (e) Different views of the PUC with triangular features whose lattice parameter is the same as in the previous case. (f) and (g) PnC waveguides with spherical and triangular features, where z is the principal wave propagation direction, and z' is a direction obtained by rotating z to 45°. The fixtures that connect the waveguides with the rest of the transducer are also shown here. $\boldsymbol{u}(\boldsymbol{l}, t)$ is the Dirichlet BC applied to these PnC waveguides at the location $\boldsymbol{l}$.

function of wave vector sampled along the IBZ, where $\boldsymbol{\Gamma}$ corresponds to the center of the BZ where the IBZ begins, i.e., at $\boldsymbol{k} = \boldsymbol{0}$. 85 eigenvalue analyses were used to represent 7 IBZ branches. We analyzed 30 wavebands in the case of the PUC with spherical features where the required BG is present between 18th and 19th bands [refer to Fig. 3(a)]. Conversely, we considered 63 bands in the case of the PUC with triangular features because of the presence of multiple BGs [refer to Fig. 3(b)], where the first BG is also between 18th and 19th bands.

Fig. 3(a) shows that by connecting spheres with rods, we can produce a wide BG of 800 kHz that spans from $f_{S1} = 700$ kHz to $f_{S2} = 1.5$ MHz, which is more than the required operating frequency range of 600 kHz. However, since the maximum overhang angle is higher than the allowable limit (45°) of 3-D printing, we could expect some variations in features (size and shape) as shown in Fig. 5(b). As all the angles in the design with triangular features are close to 45°, it is easier to fabricate with fewer variations. However, the PnC with triangular features possesses multiple narrow BGs within the operating frequency range instead of a single broad BG. The first BG of the triangular design starts at 780 kHz but only spans up to 835 kHz. The following BG spans from 880 kHz to 1.2 MHz. Nonetheless, the stacking of narrow BGs and flat modes (standing waves) goes up to 1.8 MHz with some low-slope modes present in between.

B. Transmissibility Relations

Following the band structure analysis, we study the transmissibility response of the finite PnC waveguides shown in Fig. 2. We supplied a harmonic displacement of 1 μm amplitude at the left end of each of the waveguides [as shown in Fig. 2(f) and (g)] for the frequency range from 600 kHz to 1.8 MHz with a step of 10 kHz. Fig. 4 shows transmissibility relations of waveguides obtained by taking the ratio of output displacement (right side) to the input displacement for the applied frequency range, where shaded regions represent the triangular PnC's BGs. In the same figure, the BG of the PnC with spherical features is bounded by thick black lines. As the figure shows, the BG frequency ranges are consistent with those dictated by band structure analyses. However, several peaks are present in the transmissibility relations of both designs due to the reflections from the free surfaces and subsystem resonances (i.e., the resonant modes of the finite structure within the bandgap (BG) frequency range). Band structure analysis will not capture them since the analysis is operating on a single PUC and assumes infinite material with BFPBCs. Although the band structure analysis report that the PnC with spherical features has a broader BG frequency range than that of the PnC with triangular features, the latter possesses multiple narrow BGs bounded by f_1 through f_{13} spanning almost the same frequency range as the former—and also outperforming the former in the 1.5–1.8 MHz range. However, there are still certain frequency bounds (between f_2 and f_3, between f_4 and f_5, and between f_8 and f_9) within the operational frequency range, where PnC waveguide with triangular features shows higher transmission compared to the spherical featured PnC due to the lack of BGs in those ranges. Both PnC waveguides are nevertheless manufactured since close to 1 MHz (marked as f_C in Fig. 4) their transmissibilities are in the range of −60 dB, which is desirable for the actual application.

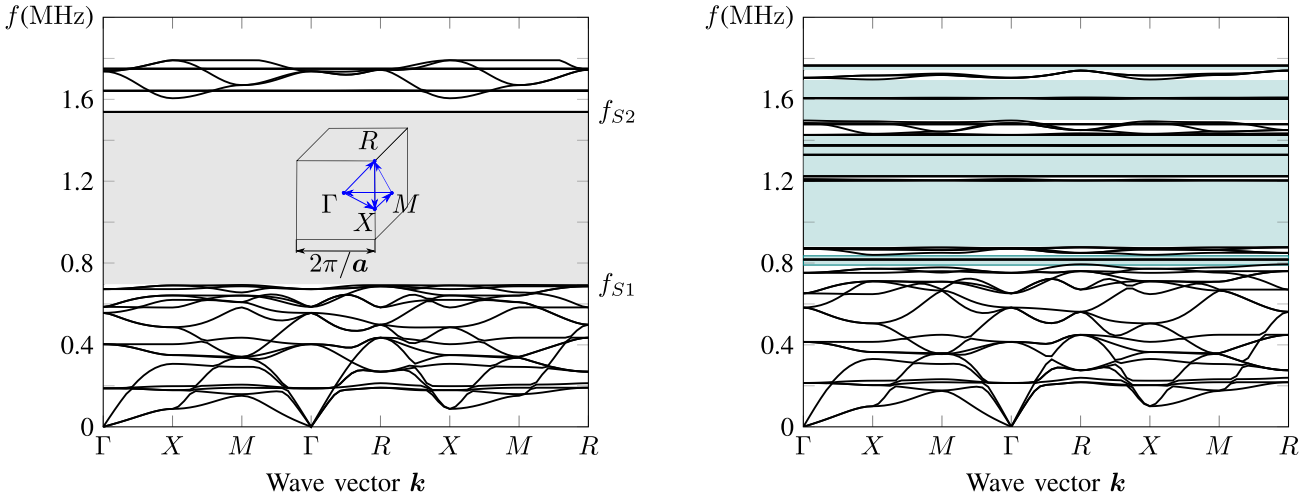

Fig. 3. Frequency as a function of wave vector (band structure) for PnCs with (a) spherical and (b) triangular internal features, where the shaded regions show corresponding BGs. $f_{S1} = 0.7$ MHz and $f_{S2} = 1.5$ MHz from (a), respectively, represent the lower and upper bound of the BG frequency ranges of the PnC with spherical features. The inset in (a) shows the BZ and its tetrahedral IBZ with its vertices.

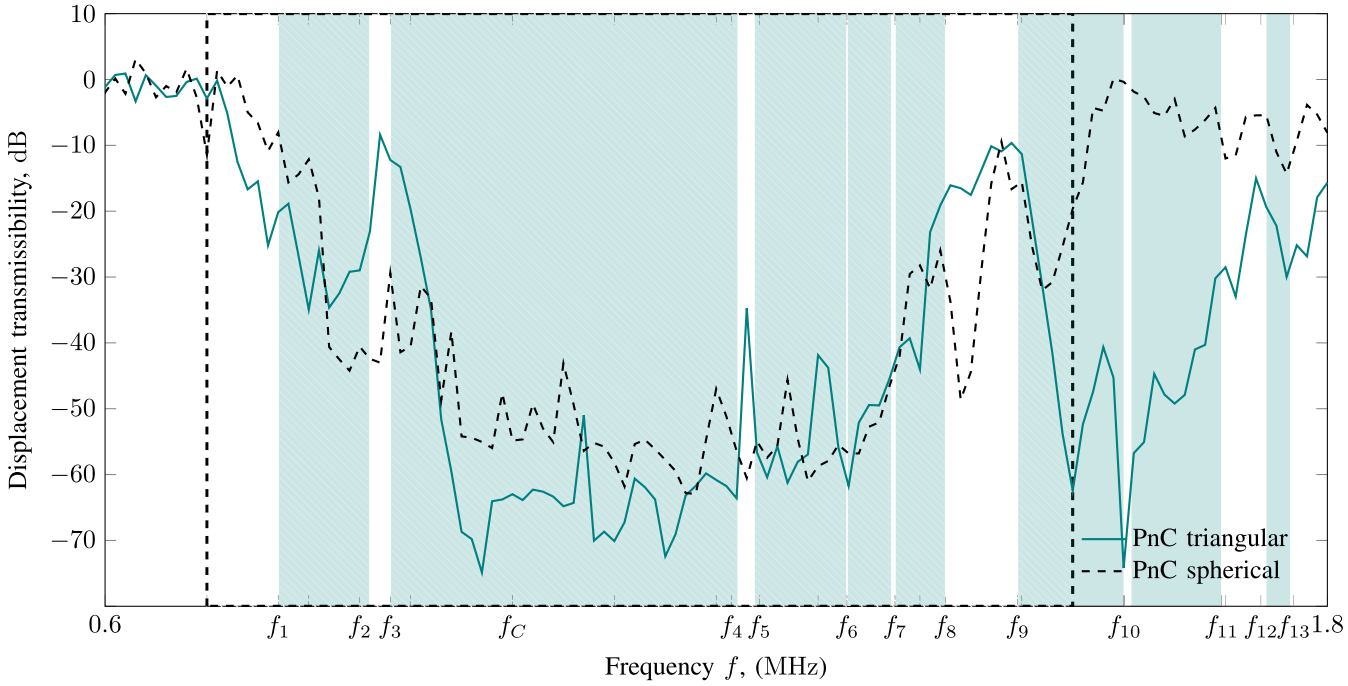

Fig. 4. Transmissibility relations of cubic PnC waveguides from Fig. 2 attained through FEM. The BG predicted by the band structure of the PnC with spherical features is bounded by thick black dashed lines, whereas shaded regions represent the BG of the PnC with triangular features. The total frequency range spans from 0.6 MHz to 1.8 MHz, where $f_C = 1$ MHz is the required central frequency and f_1 through f_{13} are frequency bounds of BGs of PnC with triangular features.

IV. Fabrication and Testing of PnC Waveguides

A. Fabrication of PnC Wave Filters

Since the dimensions of the PUC are in millimeter ranges with internal features in the submillimeter length scales, the manufacturing processes are significantly limited as mesoscale fabrication is challenging [57]. The two suitable fabrication methods are wire electric discharge machining (wire-EDM) [58] and metal additive manufacturing [59]. Although the former can produce accurate geometry, it can only remove materials from a solid block (subtractive manufacturing), limiting its applications to simpler geometries. Even though we can manufacture the PnC design from Fig. 2(g), we cannot fabricate the design from Fig. 2(f) using wire-EDM.

Metal additive manufacturing based on selective laser sintering uses laser beams to melt the metallic powder in multiple passes transforming the powder into the desired geometry. After melting every layer, more powder is added, allowing the method to generate complex designs. In addition, this method is very inexpensive compared to wire-EDM (almost two orders of magnitude). However, the accuracy

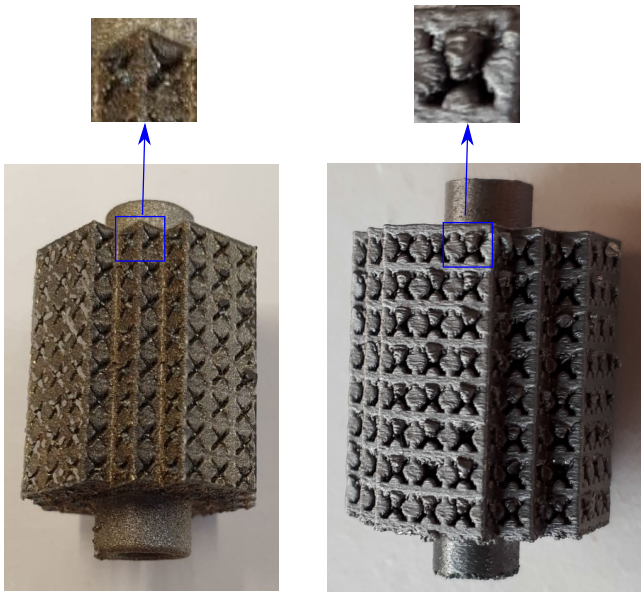

(a) (b)

Fig. 5. Photographs of 3-D printed PnC waveguides with (a) triangular and (b) spherical features. The expanded views show the corresponding PUCs, where the latter shows more variation from the model than the former.

of the fabrication depends on several factors, such as the overhang constraint, which determines the projection angle of the subsequent layer compared to the previous one, hence determining the printability and dimensional accuracy. The maximum allowable overhang angle in the metal additive manufacturing process is 45° [60]. Since the design with spherical features exceeds this angle, the surface quality, feature sizes, and shapes of the features could be adversely affected. We modified the design as described in Fig. 2(g) to minimize the overhang angles by keeping all the angles close to 45°, thereby revising the shape of the internal features (from spherical to triangular) and the printing orientation of the PnC waveguide (from aligning toward the z-direction to 45° inclination to the same direction).

B. Fabricated PnC Specimens' Variations From the Design

We decided to fabricate both designs via additive manufacturing. As shown in Fig. 5, 3-D-printed PnC specimens show certain variations from their designs. One reason is the sticking of powder particles to the sample's lower and side edges with the melt pool, thus distorting the shape. The second is because of residual support structures added to aid the printing process, which could not be removed during the post-processing stage. The PnC with spherical features also faces issues due to large overhang angles. The specimen in Fig. 5(b) has been printed by aligning the printing axis to the z-axis [refer Fig. 2(f)], whereas the specimen in Fig. 5(a) is printed by aligning the printing axis to z' by rotating it 45° from z-axis [refer Fig. 2(g)], thus keeping all the overhang angles $\leq 45°$. Consequently, the latter is more repeatable and is closer to the model.

One may wonder whether variations from the numerical model introduced by 3-D printing affect the performance of the PnC waveguide. Minor variations in feature size have insignificant effects on performance since the BG width is controlled by the mass and stiffness contrast within the PUC, which is not highly affected by slight geometric variations. Similarly, the surface roughness [as seen significantly in Fig. 5(b)] also has a minor influence on the wave attenuation behavior of the PnC waveguide as we deal with bulk waves instead of surface waves. On the contrary, if the subunit cell features (e.g., spheres) experience significant variations leading to connections between those spheres, and if there are a significant number of them, then these connection points could transmit waves leading to changes in the BG range, shifting of BG center frequency, or reduction in attenuation rate. However, as we can see in Fig. 5(a) and 5(b), this kind of distortion has not happened. As discussed, incorporating process parameters such as overhang angle greatly improves the manufacturability, as seen in the PnC with triangular features. To further improve printing accuracy, other process parameters such as layer thickness, and powder characteristics (particle size, surface tension, and feed rate), among others, can be optimized [61]; this is beyond the scope of this article. We connect both PnC waveguides with existing ultrasonic transducers and test their behavior via transient experiments. To that end, an experimental setup is built.

C. Experimental Setup to Measure the Required Signal and Crosstalk Levels of Ultrasonic Flowmeter With and Without PnC

The experimental setup for verifying the performance of the PnC waveguide is composed of PnC-mounted transducers, a signal generator for sending the desired signal, the data acquisition system (DAQ) for collecting, converting, and displaying readable data, and transducers with dummy mountings to compare the response with PnC mounted transducers to obtain the effects of the PnC. The dummy block has cross-sectional dimensions of 14 × 14 mm with a height of 16 mm. The dimensions are kept the same as that of the PnC waveguide; otherwise, the signal traveling time through the fluid would vary between those two transducers. It should be noted that the dummy block has a higher mass than the PnC waveguide since the former is a block of material, whereas the latter is a porous structure. This variation in mass will have an insignificant influence on the response of the transducer since the purpose of the dummy waveguide is to transmit the incoming elastic wave to the rest of the structure while maintaining the same construction. Both transducers (with PnC and dummy blocks) are used in pairs; one acts as a transmitter and the other as a receiver (and vice versa). The fabricated PnC waveguides (and dummy blocks) are connected to the ultrasonic transducer between the Piezo element and the transducer-wall coupling by hot pressing and welding to ensure an adequate contact [Fig. 6(a)]. A rectangular broadband pulse with a central frequency of 1 MHz and peak-to-peak voltage of 200 V is used as the input signal for the excitation. The receiving signal is amplified using a low-noise amplifier (LNA) and visualized using an oscilloscope (Yokogawa DL160) with a sampling rate of 50 MS s^{-1} and a frequency step of 500 Hz.

1) Calculation of Solid and Fluid Signal Levels: Two sets of experiments are conducted to obtain the solid and fluid signal

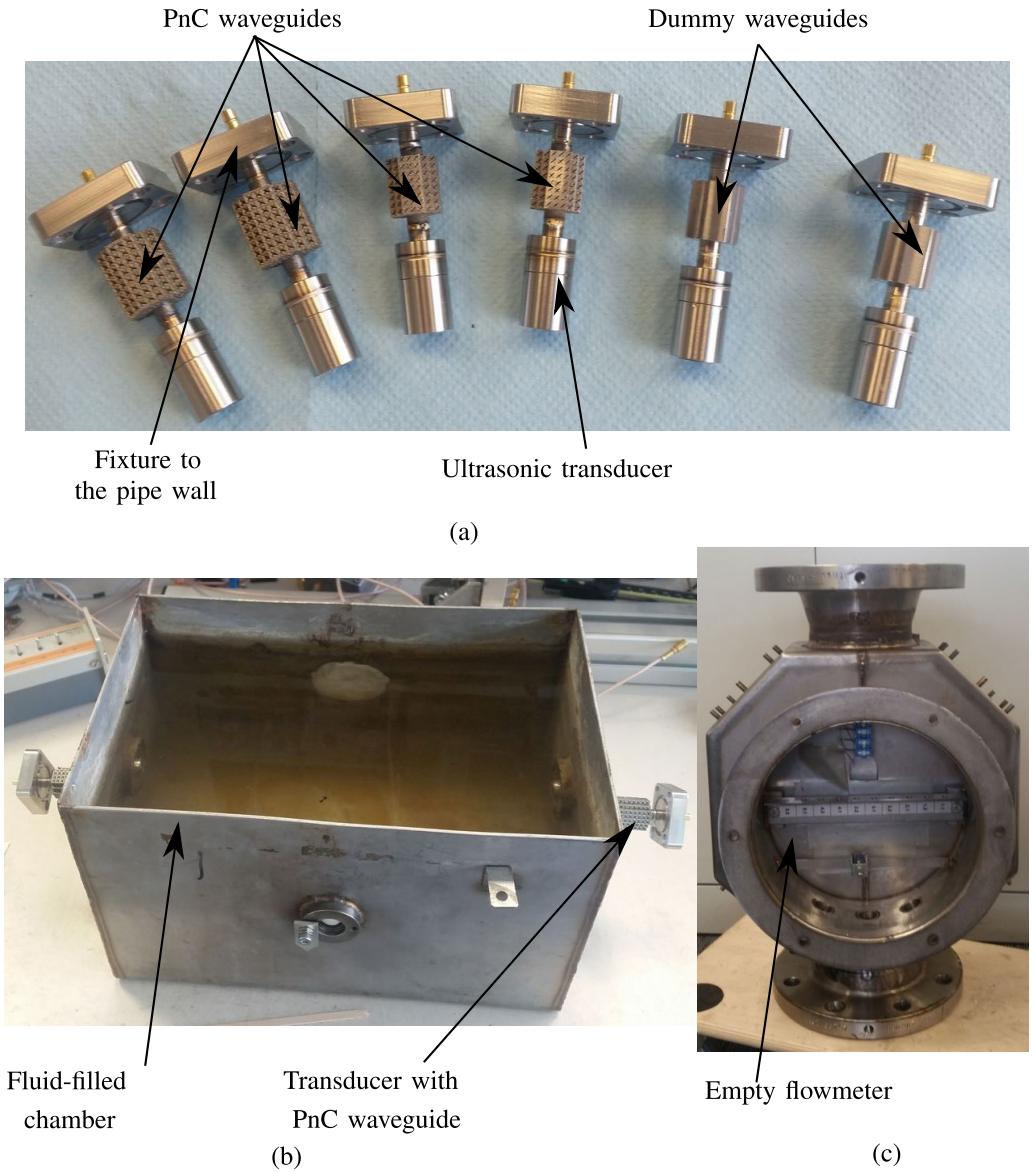

Fig. 6. Photographs of the assembled specimen and experimental setup. (a) Assembled specimens that include transducers connected with two types of PnC waveguides (PnC with spherical and triangular features) and transducers with dummy blocks. (b) Fluid-filled chamber connected with transducers to measure the signal strength in the fluid portion, whereas (c) displays the assembly of an empty flowmeter with the transducers, which is used to measure the signal levels in the solid region.

levels. The first one is performed by attaching PnC-mounted transducers to a fluid-filled chamber [as shown in Fig. 6(b)]. As the chamber walls are very thin, the energy transmitted to the solid region will also be less. In addition, since the fluid is static, the travel time for the signal through the fluid region is already known, allowing us to identify the fluid signal from the output signal, thereby measuring the required signal strength. The second one is conducted in an empty flowmeter [refer to Fig. 6(c)]. This flowmeter has a very thick solid wall, and almost all the energy from the input acoustic signal is reflected back to the solid region as there is no liquid inside. Thus the output signal can be regarded as the wall (solid) signal. The ratio of the latter signal to the former provides us with the solid-to-fluid signal ratio. The experiments are repeated with transducers possessing dummy mountings for comparison.

D. Transient Experimental Results of 3-D PnC Mounted Ultrasonic Transducers

We compare the performance of transducers with PnC wave filters against the transducer with a dummy block. Fig. 7 shows the transmissibility relations obtained by experiments. The PnC-mounted transducer shows a considerable reduction in the crosstalk level (i.e., signals traveling through the solid region are greatly attenuated) within the BG frequency range. There is an average solid-to-fluid signal reduction of 40 dB (within the BG range) and a maximum reduction of 60 dB (close to the required central frequency of 1 MHz marked as $\Delta_{S\_to\_F}$ in Fig. 7). In fact, except for 500–550 kHz (range outside the BG), both the PnC waveguides show similar performances.

From band structure analyses [refer to Fig. 3(a) and (b)], we have seen that the PnC with spherical features outperforms the PnC with triangular features due to the former's broad

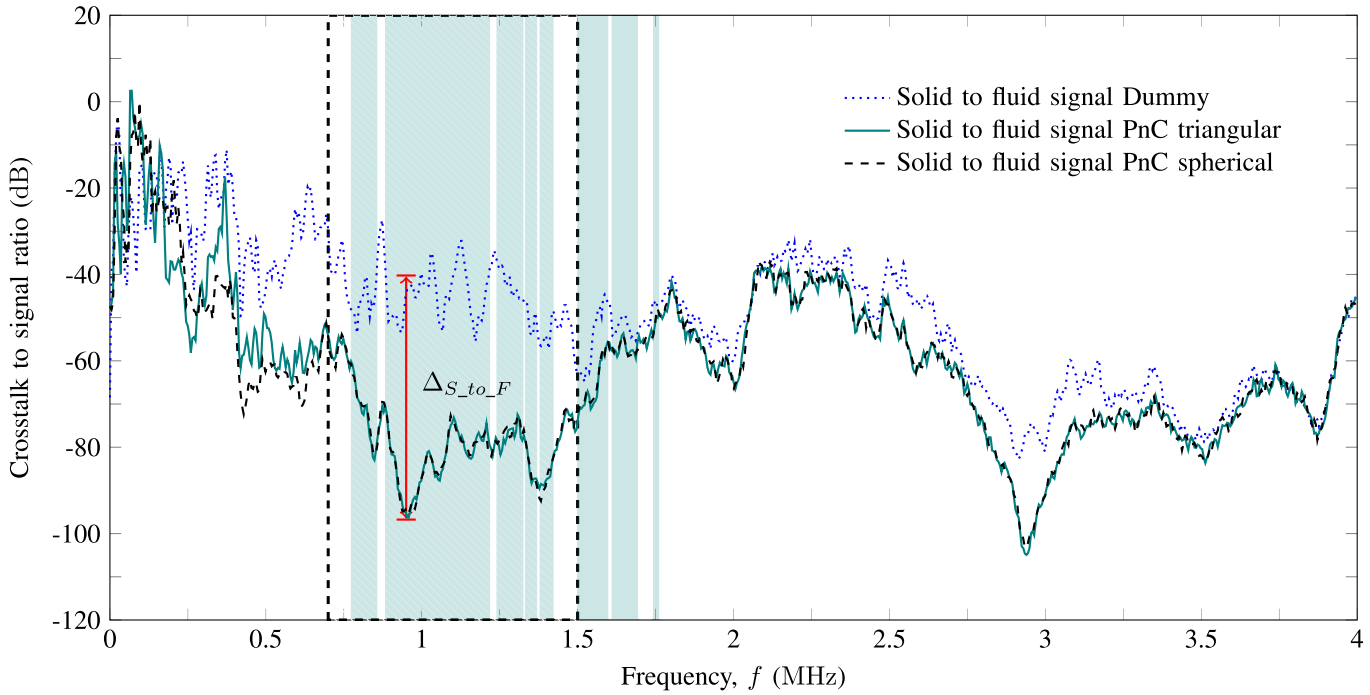

Fig. 7. Transmissibility relation of different specimens obtained via experiments. The figure includes transmissibilities of a transducer with a dummy block and transducers with triangular and spherical featured PnCs. The spherical PnC's BG is bounded by thick black lines while the triangular PnC's BG is shown using the shaded region (both predicted by analyses). $\Delta_{S\_to\_F} \approx 60$ dB represents the highest variation in the solid-to-fluid signal ratio between the transducers with and without the PnC mountings, which is observed close to the required central frequency (1 MHz).

BG as compared to a set of narrow and moderate BGs of the latter. Transmissibility analyses (refer to Fig. 4) show that the attenuation rates are closer for both the waveguides till 1.5 MHz, and the PnC with triangular features performs better than the PnC with spherical features from 1.5 to 1.8 MHz. The experiments reveal that the transmissibilities of both PnCs are very similar throughout the frequency range. The minor variations in the BG ranges and propagating modes within the operating frequency range have negligible influence on the response of wave filters. In addition, we can also observe that, even outside the BG frequency range (e.g., around 0.5, 2, 2.5, and 3 MHz), PnC-embedded transducers outperform the standard one (not as significantly as within the BG range) because of the difference in their dispersion characteristics. Especially close to 3 MHz, we can observe a sharp decrease in solid-to-fluid signal levels (about 20 dB) because of a combination of the higher-order BG generated by Bragg scattering and the high signal strength due to the presence of an actuator displacement mode at that frequency. The analysis details are discussed in the supplementary material, Section I, while the output fluid signals are provided in the supplementary material, Section II. In addition, as PnC waveguides are connected in the solid wave path, they do not influence the waves traveling through the measuring fluid; thus, the fluid signal of the PnC-embedded transducer is similar to the standard transducer (refer to supplementary material, Section II for details).

V. Conclusion

In order to improve the performance of transducers used in ultrasonic flowmeters, we proposed a mounting mechanism based on 3-D PnC waveguides. We designed two PnC wave filters, one with spherical features and the other with triangular features that facilitate additive manufacturing. While the former possesses a broad BG around the required frequency, the latter has multiple moderate and small BGs. Both were analyzed using FEA, realized via metal additive manufacturing, and mounted to the transducer by hot pressing and welding. The transient experiments showed a considerable reduction in the solid-to-fluid signal ratio within the BG frequency range (40 dB on average with a maximum of 60 dB close to 1 MHz). Thus we conclude that PnC-inspired mountings can drastically improve the measurement accuracy of ultrasonic transducers by mitigating crosstalk when connected to the solid wave path, provided the waveguides are not directly exposed to the surrounding fluid media.

Additional concluding observations are as follows.

1) Both PnC waveguides possess a frequency range of attenuation that is broader than dictated by the analysis, which implies that other factors are affecting the wave attenuation, which may be fabrication aspects (surface roughness, material constitution, variations in feature size, and shape) and structural damping.
2) Other than for a narrow frequency range, both PnC waveguides show similar transmissibility responses throughout the spectrum. Hence, it is not required to have a single broad BG, but combinations of narrow BGs, flat wave modes, and shallow-slope wave modes can add to a moderate BG to create a cumulative wave attenuation region similar to the response of a PnC with a single broad BG.

3) Throughout the frequency range except close to 100 kHz, both PnC-embedded transducers show lower solid-to-fluid signal levels compared to the standard one. This behavior could be due to the complex dispersion characteristics (varying wave speeds and combinations of different wave modes throughout the frequency range) of PnC wave filters augmented by imperfections in their manufacturing.
4) Since both spherical and triangular PnC waveguides show similar performances, we can select the latter for practical applications since they are more amenable to additive manufacturing than the former. In addition, triangular PnC waveguides can be fabricated via multiple processes (3-D printing and EDM), further improving their applicability.

PnC waveguides in real applications of ultrasonic flowmeters introduce environmental conditions such as the effects of surrounding fluid media, pressure, and temperature. Thus, a future direction could be to perform an optimization of PnC-inspired mountings incorporating multiple environmental aspects.

ACKNOWLEDGMENT

The authors extend their appreciation to Dr. Jankees Hogendoorn, Jeroen van Klooster, Rogier Geerders, and Arie Huijzer from KROHNE Altometer, Dordrecht, The Netherlands, for their extensive support in the experimentation.

REFERENCES

[1] L. Lynnworth and Y. Liu, "Ultrasonic flowmeters: Half-century progress report, 1955–2005," *Ultrasonics*, vol. 44, pp. e1371–e1378, Dec. 2006. [Online]. Available: https://www.sciencedirect.com/science/article/pii/S0041624X06000849

[2] D. L. Franklin, D. W. Baker, R. M. Ellis, and R. F. Rushmer, "A pulsed ultrasonic flowmeter," *IRE Trans. Med. Electron.*, vol. ME-6, no. 4, pp. 204–206, 1959.

[3] P. I. Moore, G. J. Brown, and B. P. Stimpson, "Ultrasonic transit-time flowmeters modelled with theoretical velocity profiles: Methodology," *Meas. Sci. Technol.*, vol. 11, no. 12, pp. 1802–1811, Nov. 2000, doi: 10.1088/0957-0233/11/12/321.

[4] G. Rajita and N. Mandal, "Review on transit time ultrasonic flowmeter," in *Proc. 2nd Int. Conf. Control, Instrum., Energy Commun. (CIEC)*, Jan. 2016, pp. 88–92.

[5] J. Blitz and G. Simpson, *Ultrasonic Methods of Non-Destructive Testing*, vol. 2. Cham, Switzerland: Springer, 1995.

[6] J. Helal, M. Sofi, and P. Mendis, "Non-destructive testing of concrete: A review of methods," *Electron. J. Struct. Eng.*, vol. 14, no. 1, pp. 97–105, 2015.

[7] S. Chatillon, G. Cattiaux, M. Serre, and O. Roy, "Ultrasonic non-destructive testing of pieces of complex geometry with a flexible phased array transducer," *Ultrasonics*, vol. 38, nos. 1–8, pp. 131–134, Mar. 2000.

[8] J. F. Havlice and J. C. Taenzer, "Medical ultrasonic imaging: An overview of principles and instrumentation," *Proc. IEEE*, vol. 67, no. 4, pp. 620–641, 1979.

[9] P. Abolmaesumi, S. E. Salcudean, W.-H. Zhu, M. R. Sirouspour, and S. P. DiMaio, "Image-guided control of a robot for medical ultrasound," *IEEE Trans. Robot. Autom.*, vol. 18, no. 1, pp. 11–23, 2002.

[10] J. Powers and F. Kremkau, "Medical ultrasound systems," *Interface Focus*, vol. 1, no. 4, pp. 477–489, Aug. 2011.

[11] J. Hogendoorn, K. Tawackolian, P. van Brakel, J. van Klooster, and J. Drenthen, "High viscosity hydrocarbon flow measurement: A challenge for ultrasonic flow meters?" in *Proc. 27th Int. North Sea Flow Meas. Workshop*, 2009, pp. 1–20.

[12] P. Ueberschlag, A. Berger, and M. Bezdek, "Ultrasonic transducer for application in an ultrasonic, flow measuring device or in an ultrasonic, fill-level measuring device," U.S. Patent 10 620 026, Apr. 14, 2020.

[13] E. J. Gottlieb, K. P. Minnock, D. R. Augenstein, and R. A. Zuckerman, "Acoustically isolated ultrasonic transducer housing and flow meter," U.S. Patent 9 506 789, Nov. 29, 2016.

[14] J. M. Van Klooster, "Flowmeter," U.S. Patent 6 799 475, Oct. 5, 2004.

[15] S. T. Nielsen, P. S. Laursen, and J. L. Sørensen, "Flow meter with protruding transducers," U.S. Patent 9 182 260, Nov. 10, 2015.

[16] A. Ramos, J. L. San Emeterio, and P. T. Sanz, "Improvement in transient piezoelectric responses of NDE transceivers using selective damping and tuning networks," *IEEE Trans. Ultrason., Ferroelectr. Freq. Control*, vol. 47, no. 4, pp. 826–835, Jul. 2000.

[17] J. M. Van Klooster and A. Huijzer, "Ultrasonic transducer," U.S. Patent 8 127 613, Mar. 6, 2012.

[18] D. Zheng, P. Zhang, and T. Xu, "Study of acoustic transducer protrusion and recess effects on ultrasonic flowmeter measurement by numerical simulation," *Flow Meas. Instrum.*, vol. 22, no. 5, pp. 488–493, Oct. 2011.

[19] Y. Hu, T. Zhang, and D. Zheng, "Estimation on influence of probe protrusion length of ultrasonic flowmeter on measurement," *J. Tianjin Univ.*, vol. 46, no. 9, pp. 776–783, 2013.

[20] L. C. Lynnworth, "Ultrasonic transducer system with crosstalk isolation," U.S. Patent 5 515 733, May 14, 1996.

[21] M. S. Kushwaha, P. Halevi, L. Dobrzynski, and B. Djafari-Rouhani, "Acoustic band structure of periodic elastic composites," *Phys. Rev. Lett.*, vol. 71, pp. 2022–2025, Sep. 1993.

[22] M. S. Kushwaha, P. Halevi, G. Martínez, L. Dobrzynski, and B. Djafari-Rouhani, "Theory of acoustic band structure of periodic elastic composites," *Phys. Rev. B, Condens. Matter*, vol. 49, no. 4, pp. 2313–2322, Jan. 1994.

[23] P. Deymier, *Acoustic Metamaterials Phononic Crystals*, (Springer Series in Solid-State Sciences). Berlin, Germany: Springer, 2013. [Online]. Available: https://books.google.nl/books?id=8eg_AAAAQBAJ

[24] W. L. Bragg, "The diffraction of short electromagnetic waves by a crystal," *Scientia*, vol. 23, no. 45, p. 153, 1929.

[25] M. Reynolds and S. Daley, "An active viscoelastic metamaterial for isolation applications," *Smart Mater. Struct.*, vol. 23, no. 4, Apr. 2014, Art. no. 045030.

[26] K. H. Sun, J. E. Kim, J. Kim, and K. Song, "Sound energy harvesting using a doubly coiled-up acoustic metamaterial cavity," *Smart Mater. Struct.*, vol. 26, no. 7, Jul. 2017, Art. no. 075011.

[27] S. Zhang, C. Xia, and N. Fang, "Broadband acoustic cloak for ultrasound waves," *Phys. Rev. Lett.*, vol. 106, no. 2, Jan. 2011, Art. no. 024301.

[28] C. M. Park, J. J. Park, S. H. Lee, Y. M. Seo, C. K. Kim, and S. H. Lee, "Amplification of acoustic evanescent waves using metamaterial slabs," *Phys. Rev. Lett.*, vol. 107, no. 19, Nov. 2011, Art. no. 194301.

[29] G. Y. Song, B. Huang, H. Y. Dong, Q. Cheng, and T. J. Cui, "Broadband focusing acoustic lens based on fractal metamaterials," *Sci. Rep.*, vol. 6, no. 1, p. 35929, Oct. 2016.

[30] J. Xu and J. Tang, "Tunable prism based on piezoelectric metamaterial for acoustic beam steering," *Appl. Phys. Lett.*, vol. 110, no. 18, May 2017, Art. no. 181902.

[31] W. A. Smith, A. Shaulov, and B. A. Auld, "Tailoring the properties of composite piezoelectric materials for medical ultrasonic transducers," in *Proc. IEEE Ultrason. Symp.*, Jan. 1985, pp. 642–647.

[32] W. A. Smith and B. A. Auld, "Modeling 1–3 composite piezoelectrics: Thickness-mode oscillations," *IEEE Trans. Ultrason., Ferroelectr., Freq. Control*, vol. 38, no. 1, pp. 40–47, Jan. 1991.

[33] W. A. Smith, "The role of piezocomposites in ultrasonic transducers," in *Proc. IEEE Proceedings. Ultrason. Symp.*, Feb. 1989, pp. 755–766.

[34] W. A. Smith and A. A. Shaulov, "Composite piezoelectrics: Basic research to a practical device," *Ferroelectrics*, vol. 87, no. 1, pp. 309–320, Nov. 1988, doi: 10.1080/00150198808201393.

[35] M. Miniaci et al., "Proof of concept for an ultrasensitive technique to detect and localize sources of elastic nonlinearity using phononic crystals," *Phys. Rev. Lett.*, vol. 118, May 2017, Art. no. 214301. [Online]. Available: https://link.aps.org/doi/10.1103/PhysRevLett.118.214301

[36] E. J. Smith and K. H. Matlack, "Metal additively manufactured phononic materials as ultrasonic filters in nonlinear ultrasound measurements," *J. Acoust. Soc. Amer.*, vol. 149, no. 6, pp. 3739–3750, Jun. 2021, doi: 10.1121/10.0004995.

[37] M. Liu et al., "Applications of a nanocomposite-inspired in-situ broadband ultrasonic sensor to acousto-ultrasonics-based passive and active structural health monitoring," *Ultrasonics*, vol. 78, pp. 166–174, 2017. [Online]. Available: https://www.sciencedirect.com/science/article/pii/S0041624X16302414

[38] M. Kabir, A. Mostavi, and D. Ozevin, "Noise isolation with phononic crystals to enhance fatigue crack growth detection using acoustic emission," *J. Civil Structural Health Monitor.*, vol. 8, no. 3, pp. 529–542, Jul. 2018.

[39] X. Li, "A brief review: Acoustic emission method for tool wear monitoring during turning," *Int. J. Mach. Tools Manuf.*, vol. 42, no. 2, pp. 157–165, Jan. 2002. [Online]. Available: https://www.sciencedirect.com/science/article/pii/S0890695501001080

[40] P. Ji, W. Hu, and J. Yang, "Development of an acoustic filter for parametric loudspeaker using phononic crystals," *Ultrasonics*, vol. 67, pp. 160–167, Apr. 2016. [Online]. Available: https://www.sciencedirect.com/science/article/pii/S0041624X16000147

[41] G. R. Sherwood, D. Chronopoulos, A. Marini, and F. Ciampa, "3D-printed phononic crystal waveguide transducers for nonlinear ultrasonic damage detection," *NDT & E Int.*, vol. 121, Jan. 2021, Art. no. 102456. [Online]. Available: https://www.sciencedirect.com/science/article/pii/S0963869521000554

[42] R. Baker, *Flow Measurement Handbook* (Flow Measurement Handbook: Industrial Designs, Operating Principles, Performance, and Applications). Cambridge, U.K.: Cambridge Univ. Press, 2016. [Online]. Available: https://books.google.nl/books?id=D4-5DAAAQBAJ

[43] J. S. Wilson, *Sensor Technology Handbook*. Amsterdam, The Netherlands: Elsevier, 2004.

[44] R. M. Martin, "Piezoelectricity," *Phys. Rev. B, Condens. Matter*, vol. 5, pp. 1607–1613, Feb. 1972. [Online]. Available: https://link.aps.org/doi/10.1103/PhysRevB.5.1607

[45] N. Roosnek, "Novel digital signal processing techniques for ultrasonic gas flow measurements," *Flow Meas. Instrum.*, vol. 11, no. 2, pp. 89–99, Jun. 2000.. [Online]. Available: https://www.sciencedirect.com/science/article/pii/S095559860000008X

[46] K. F. Graff, *Wave Motion in Elastic Solids*. North Chelmsford, MA, USA: Courier Corporation, 2012.

[47] A. Bedford and D. Drumheller, *Elastic Wave Propagation*. Hoboken, NJ, USA: Wiley, 1994, pp. 151–165.

[48] F. Bloch, "Quantum mechanics of electrons in crystal lattices," *Z, Phys.*, vol. 52, pp. 555–600, Jan. 1928.

[49] H. J. Monkhorst and J. D. Pack, "Special points for Brillouin-zone integrations," *Phys. Rev. B, Condens. Matter*, vol. 13, no. 12, pp. 5188–5192, Jun. 1976, doi: 10.1103/PhysRevB.13.5188.

[50] C. Kittel and P. McEuen, *Introduction to Solid State Physics*. Hoboken, NJ, USA: Wiley, 2018.

[51] L. P. Bouckaert, R. Smoluchowski, and E. Wigner, "Theory of Brillouin zones and symmetry properties of wave functions in crystals," *Phys. Rev.*, vol. 50, pp. 58–67, Jul. 1936. [Online]. Available: https://link.aps.org/doi/10.1103/PhysRev.50.58

[52] Y. Chen, H. Yao, and L. Wang, "Acoustic band gaps of three-dimensional periodic polymer cellular solids with cubic symmetry," *J. Appl. Phys.*, vol. 114, no. 4, Jul. 2013, Art. no. 043521, doi: 10.1063/1.4817168.

[53] I. L. Vér and L. L. Beranek, *Noise and Vibration Control Engineering: Principles and Applications*. Hoboken, NJ, USA: Wiley, 2005.

[54] T. J. Hughes, *The Finite Element Method: Linear Static and Dynamic Finite Element Analysis*. North Chelmsford, MA, USA: Courier Corporation, 2012.

[55] M. Hirsekorn, P. P. Delsanto, N. K. Batra, and P. Matic, "Modelling and simulation of acoustic wave propagation in locally resonant sonic materials," *Ultrasonics*, vol. 42, nos. 1–9, pp. 231–235, Apr. 2004. [Online]. Available: https://www.sciencedirect.com/science/article/pii/S0041624X04000216

[56] L. D'Alessandro, E. Belloni, R. Ardito, A. Corigliano, and F. Braghin, "Modeling and experimental verification of an ultra-wide bandgap in 3D phononic crystal," *Appl. Phys. Lett.*, vol. 109, no. 22, Nov. 2016, Art. no. 221907, doi: 10.1063/1.4971290.

[57] G. L. Benavides, D. P. Adams, and P. Yang, "Meso-machining capabilities," Sandia Nat. Laboratories, Albuquerque, New Mexico, Tech. Rep., SAND2001-1708, 2001.

[58] Y. S. Liao, J. T. Huang, and Y. H. Chen, "A study to achieve a fine surface finish in wire-EDM," *J. Mater. Process. Technol.*, vol. 149, nos. 1–3, pp. 165–171, Jun. 2004. [Online]. Available: https://www.sciencedirect.com/science/article/pii/S0924013604001463,keywords=Wire-EDM,Finish,Pulse-generatingcircuit,Surfaceroughness

[59] W. E. Frazier, "Metal additive manufacturing: A review," *J. Mater. Eng. Perform.*, vol. 23, no. 6, pp. 1917–1928, 2014, doi: 10.1007/s11665-014-0958-z.

[60] S. Feng, A. M. Kamat, S. Sabooni, and Y. Pei, "Experimental and numerical investigation of the origin of surface roughness in laser powder bed fused overhang regions," *Virtual Phys. Prototyping*, vol. 16, no. 1, pp. S66–S84, 2021, doi: 10.1080/17452759.2021.1896970.

[61] H. Fayazfar et al., "A critical review of powder-based additive manufacturing of ferrous alloys: Process parameters, microstructure and mechanical properties," *Mater. Design*, vol. 144, pp. 98–128, Jan. 2018. [Online]. Available: https://www.sciencedirect.com/science/article/pii/S0264127518300972

Sabiju Valiya Valappil was born in Kerala, India. He received the master's degree in mechanical systems design from the Indian Institute of Technology Kharagpur, India, in 2014. He is currently pursuing the Ph.D. degree with the Department of Precision and Microsystems Engineering, Faculty of Mechanical, Maritime and Materials Engineering, Delft University of Technology, Delft, The Netherlands.

His research interests include phononic crystals and acoustic metamaterials, elastic and acoustic wave propagation, structural dynamics, and numerical modeling.

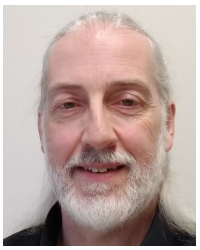

Johannes F. L. Goosen was born in Rotterdam, The Netherlands, in 1966. He received the master's degree in electronic engineering from the Delft University of Technology, The Netherlands, in 1991, and the Ph.D. degree in 1996, for his thesis called "Design and fabrication of a surface micromachined positioning device."

After four years as a Post-Doctoral Researcher on the development of miniature sensors for catheters, he is currently working as an Assistant Professor at the Precision and Microsystems Engineering Department, Faculty of Mechanical, Maritime and Materials Engineering, Delft University of Technology. He leads a group focusing on high-level system and function integration, miniaturization, and their links to manufacturing. He was a Founding Member of the MicroNed National Research Program and has led several collaborative research projects. Current efforts are directed at metamaterial-based functions, micro-robotics, and mesoscale manufacture.

Alejandro M. Aragón was born in San Juan, Argentina. He received the M.Sc. (Fulbright Scholarship) and Ph.D. degrees from the University of Illinois at Urbana-Champaign (UIUC), IL, USA, in 2006 and 2010, respectively.

After two post-doctorate appointments (UIUC and EPFL, Lausanne, Switzerland), in 2014, he became a Faculty Member with the Delft University of Technology, The Netherlands. He is currently an Associate Professor with the Precision and Microsystems Engineering Department, Mechanical Engineering Faculty. He is leading a group focusing on developing novel finite element technologies for the computational analysis and design of (meta)materials and structures. These techniques have been used for tailoring the fracture resistance of brittle solids, the design of phononic/photonic devices, and efficient contact modeling, among others.